Composites Part B 300 (2025) 112483

Contents lists available at ScienceDirect

Composites Part B

journal homepage: www.elsevier.com/locate/compositesb

Model based assessment of maximal surface temperatures and heat flow in edge trimming of UD CFRP with tools of different type

Wolfgang Hintze, Ganna Shchegel *, Jan Mehnen, Carsten Möller, Jan Dege

Institute of Production Management and Technology, Hamburg University of Technology, Denickestraße 17, 21073, Hamburg, Germany

ARTICLE INFO

Handling Editor: Prof. Ole Thomsen

Keywords:
CFRP
Milling
Moving heat source
Surface damage
Temperature
Heat flow
Fibre orientation angle

ABSTRACT

Excessive heating during edge trimming of CFRP components leads to matrix degradation impairing their quality. The thermal response of unidirectional CFRP when machining with different tool types is studied: PCD cutters, coated carbide routers, and diamond grinding pins. Temperature and torque were measured at various fibre orientation angles Φ and cutting conditions. Based on an analytical model, key thermal parameters were identified from experimental data. For all tools, temperatures exceeded the matrix glass transition temperature under most conditions. Maximum of temperature changes was observed at $\Phi = 135°$, minimum at $\Phi = 90°$ was most pronounced for the cutter, less noticeable for the router, and almost absent for the grinding pin. At $\Phi = 90°$, the thermal contact length and heat flow ratio typically reached maximum values, while the heat flux was at its lowest. Regarding cutting conditions for both the cutter and router, an increase in cutting speed led to higher equivalent heat flux, heat flow, and temperature change. In contrast, for grinding pins, temperature change increased at the lower cutting speed or feed rate. In grinding, heat flow, equivalent heat flux and thermal contact length were primarily influenced by the fibre orientation symmetry angle, whereas heat flow and equivalent heat flux were nearly independent of the cutting conditions. Thus, the tool types exhibit different thermal parameters and patterns of their dependencies on the machining conditions, which are differentiated by the model and can be explained by pulsed point, pulsed linear or continuous surface contact of individual cutting edges.

1. Introduction and state of the art

The use of carbon fibre-reinforced plastics (CFRP) offers one of the most effective solutions in lightweight engineering, particularly in applications where a high strength-to-weight ratio is crucial. This advantage is especially significant in aviation, as well as in ground and water vehicles, where the use of CFRP plays a key role in reducing fuel consumption and, consequently, CO_2 emissions.

Fibre reinforcement influences not only the material's behavior in finished components but also its response during mechanical processing in production. One critical aspect is that it determines the predominant directions of heat flow and the resulting temperature distribution during the machining of composite components [1]. This effect is particularly evident in trimming, a necessary step after CFRP consolidation to achieve precise geometric contours and high surface quality in manufactured parts [2,3].

As extensively studied in Refs. [4–8], research indicates that during typical machining processes, surface temperatures may exceed the glass transition temperature T_g and even the thermal decomposition temperature of the epoxy matrix. Exceeding T_g leads to a severe deterioration of the matrix's mechanical properties and its ability to support the fibres, the loss of fibre support results in poor surface integrity and delamination, which can act as stress concentrators and initiate crack propagation under loading [9–13].

Some studies focus on the influence of tool types used in machining on the temperatures generated during the process [5,6,14]. Contour processing of thin-walled CFRP structures can be performed using various tool types.

One group of tools, such as peripheral milling cutters of defined geometry, enables material removal through a cutting process, where the number of cutting edges and the tool's micro- and macrogeometry are precisely known. The influence of cutting parameters on machining quality has been investigated in Refs. [15–18].

Another group of tools provides an abrasive machining process using fixed abrasive particles, where the geometric characteristics of the cutting edges can only be described statistically. An example of such tools is grinding pins, which have a small diameter-to-working-length ratio along the axial direction and are suitable for trimming curved contours [19].

* Corresponding author.
E-mail address: ganna.shchegel@tuhh.de (G. Shchegel).

https://doi.org/10.1016/j.compositesb.2025.112483
Received 7 February 2025; Received in revised form 26 March 2025; Accepted 2 April 2025
Available online 4 April 2025

Nomenclature

$a_{e,eff}$	effective width of cut
$a_{e,nom}$	nominal width of cut
a_p	depth of cut equal to thickness of the tested CFRP-panels
C_p	specific heat capacity
d_t	tool diameter
f	feed
h	chip thickness
K_0	modified Bessel function of the second kind of order zero
k_{11}	thermal conductivity in 1st orthotropic direction parallel to fibres
k_{33}	thermal conductivity in 2nd orthotropic direction perpendicular to fibres
n	number of spindle revolutions per unit time
l_m	length of machined path
P_c	cutting power
P_{HS}	heat flow into the workpiece
q_{HS}	equivalent heat flux of the heat source
r_β	radius of the tool cutting-edge
R_W	ratio of the heat flow from the heat source into the workpiece to the cutting power
s_{HS}	thermal contact length of the heat source
T_g	glass transition temperature
v_c	cutting speed
v_f	feed rate and heat source velocity
x_{HS}	horizontal position of the centre of the heat source
x_n	horizontal coordinate of the point of interest for which the temperature is modeled
z_i	distance from the machined surface to the thermographic camera measurement line
z_n	vertical coordinate of the point of interest for which the temperature is modeled
α_f	tool clearance angle
γ_f	tool rake angle
δ	tool helix angle
Δa_e	relative change of the width of cut
ΔT_{max}	maximum temperature change
ζ_Φ	fibre orientation symmetry angle
θ	fibre cutting angle
ρ_w	density
Φ	fibre orientation angle
φ	tool engagement angle

Cutting processes can also be performed using routers, which, due to their high number of defined cutting edges, help mitigate abrupt dynamic effects caused by cutting edge entry and exit. From this perspective, such processes share similarities with grinding pin operations, which are characterized by a steady engagement [19,20].

The choice between these tool types plays a crucial role in the temperature increase of both the tool and the workpiece [20].

In [5], it was found that when tested at the same feed per revolution, a polycrystalline diamond (PCD) peripheral milling cutter with two cutting teeth and a diamond-coated router led to similar simulated cutting temperatures, which were higher compared to those of a TiAlN-coated router. The simulation was based on measurements obtained using thermocouples embedded in the workpiece and an infrared camera.

A similar experimental setup, but involving side measurement of temperatures on the lateral surface of the processed panel, was used in Ref. [21]. This approach allowed for temperature measurements closer to the tool-material interaction region. Therefore, it addressed the issue of heat dissipation into the surroundings, which contributes to lower measured temperatures at greater distances from the interaction zone and may lead to an underestimation of the actual temperature at the machined surface.

According to Ref. [6], an uncoated carbide cutter with four helix flutes generated slightly lower temperatures in trimming compared to a similar coated carbide cutter and a two-tooth straight PCD tool. However, in this study, the panels consisted of CFRP and Ti6Al4V stacks, meaning the results were influenced by the presence of titanium alloy layers.

In [14], a one-tooth uncoated straight cutter was examined. It was shown that negative rake angles, which are also characteristic of the cutting grains in abrasive tools, lead to significantly higher temperatures in CFRP trimming.

The objective of the present study is to address the lack of a systematic comparison of CFRP's thermal response in trimming using different tool types. This research focuses on three tools widely used in industrial manufacturing: a cutter, a router, and a grinding pin.

Concerning the influence of machining conditions [7], demonstrated that in CFRP trimming, an increase in cutting speed is the key parameter leading to higher process temperatures. Additionally, an increase in feed rate also resulted in slightly higher temperatures immediately in the cutting region, as indicated by tool-workpiece thermocouple temperature measurements.

According to the measurements in Ref. [10], the temperature at the machined CFRP surface rises with increasing cutting speed. However, at certain distances from the machined surface, the temperature decreases when both cutting speed and feed rate increase, provided that the feed per tooth remains constant. Results in Refs. [2,5] confirm that temperatures tend to decrease with increasing feed rate when measured at some distance from the tool-workpiece contact region, as observed in Ref. [5], or within the tool itself, as seen in Ref. [2]. The latter effect can be attributed to better heat dissipation due to the interaction with still non-heated material regions when moving at higher feed rates.

The findings in Ref. [21] further support the same conclusions regarding temperature dependency at the machined surface. These results were obtained by measuring temperatures at small distances from the tool-workpiece contact region while utilizing an analytical temperature field model adapted for orthotropic CFRP panels, as described in Ref. [1]. This model enables a reasonable extrapolation of the measured temperature to the machined surface, eliminating the need for special CFRP layers or modifications to the tool-side test setup to accommodate a tool-workpiece thermocouple, which could potentially influence temperature readings.

The primary objective of this study is explicitly realized through a detailed analysis and comparison of key thermal response parameters, including heat flux, heat source length, heat flow, and the ratio of heat flow to cutting power. These parameters will be introduced and explained in detail in the following sections. They are determined for the trimming of identical CFRP panels under various processing conditions, such as.

- constant feed per revolution with varying cutting speeds,
- constant cutting speed with varying feeds per revolution and widths of cut,
- constant material removal rate with varying other conditions.

To achieve this, the study leverages the experimental and modeling approach described in Ref. [21].

Temperature development is often studied in the context of unidirectional (UD) CFRP, where fibres throughout the laminate's thickness are aligned in a single primary direction within the panel plane. This

direction defines the main orthotropy axis of the CFRP panel, while the second orthotropy direction lies perpendicular to it within the panel plane. The findings from such studies can be adopted to individual UD layers in non-crimp fabrics, which are widely used due to their excellent mechanical, chemical, and thermal properties, enhancing the composite's overall mechanical performance.

The fibre orientation angle is defined as the angle between the positive direction of the feed rate vector and the fibre direction on the bulk side of the processed fibre-reinforced workpiece (as opposed to its cut-off side). Studies on the temperature response of UD-CFRP have demonstrated a high sensitivity of the temperature field to the fibre orientation angle, with maximum temperatures observed at $\Phi = 135°$ [20–22].

An important objective of this research is to analyze the dependency of the thermal response on the orthotropic direction of the composite material. This is achieved by investigating its correlation with the workpiece's fibre orientation angle. To this end, an analytical model, as described in Ref. [1], was employed to analyze temperature fields and heat transfer during the machining of orthotropic composites with arbitrary fibre orientations. The model incorporates the fibre orientation angle as a parameter in a general equation, which relates the workpiece temperature to heat flux and machining parameters for any given fibre orientation angle [1].

The model addresses the heat transfer problem in CFRP as a steady-state heat conduction process in an orthotropic solid. It treats the tool-material interaction region as a moving heat source, with the temperature field in the workpiece described by the classical heat equation, incorporating boundary conditions that account for heat flux from the cutting zone [22–24]. The analytical model in Ref. [1] is an extension of the model of the moving heat source for the case of an isotropic solid, which was described in Ref. [23] and extensively used in thermal cutting modeling [25–27]. Within the framework of the inverse heat conduction problem, and considering that temperature measurement is more feasible than direct heat flux measurement, temperature data from the workpiece are used to estimate heat flux [28,29].

The model utilized incorporates two key parameters for representing a tool as a moving heat source: the thermal contact length s_{HS} and the equivalent heat source flux q_{HS} [1]. This model can be employed to empirically determine the key thermal parameters of the edge trimming process through laboratory experiments. Depending on these parameters, and under conditions of the same total heat flow P_{HS}, the resulting temperature can vary significantly [30].

In general, additional material heating or, conversely, the application of cooling agents or the consideration of non-adiabatic process boundary conditions, both can be accounted for by introducing additional positive or negative heat fluxes q_{HS}. However, this aspect was beyond the scope of the present study.

To summarize, the interaction between tool types and processing parameters, such as cutting speed v_c, feed f, width of cut a_e, and fibre orientation angle Φ, plays a crucial role in temperature development during the machining of UD-CFRP. This research aims to bridge the existing knowledge gap regarding their influence on the formation of the CFRP thermal response in trimming.

2. Materials and methods

Edge trimming experiments were performed using three different tools on UD-CFRP panels with varying fibre orientation angle Φ. Subsequently, the temperature field was simulated based on the workpiece temperatures measured during machining.

2.1. Scheme of experiment

Vertically mounted CFRP plates were trimmed along their upper edge in full (nominal width of cut $a_{e,nom}$ is equal to the tool diameter d_t, $a_{e,nom} = d_t$) and partial ($a_{e,nom} < d_t$) cuts in up-cut milling. The scheme of the experiment is shown in Fig. 1.

The fibre direction of the prepared plates on the bulk side of the trimmed panel (opposite to the cut-off side) and the feed rate vector v_f define the fibre orientation angle Φ. The workpiece is clamped at the bottom using a robust metallic traverse, securely fastened with a set of uniformly distributed clips along its length. The longitudinal axis of the tool is oriented perpendicular to the (x,z) plane.

Table 1 provides the numerical values for the experimental setup configuration and the parameters of the tools used.

2.2. Tools

The tools used in the tests included two cutting tools of defined geometry and one abrasive tool, as shown in Fig. 2.

Double-edged polycrystalline diamond (PCD) cutter (Fig. 2a): this cutting tool featured a cemented carbide shaft and was characterized by rake angle $\gamma_f = 0°$, helix angle $\delta = 0°$, and clearance angle $\alpha_f = 12°$.

Diamond-coated right-hand (clockwise rotating) router (Fig. 2b): this cutting tool had ten cutting teeth arranged circumferentially with a clockwise axial shift of adjacent tooth rows.

Diamond-coated grinding pin (Fig. 2c): this abrasive tool featured a galvanic bond and coarse diamond grit D427.

All tools were used in a work-sharp state. The cutting region of each tool was shifted axially along the cantilever length in multiple steps, ensuring that the total length of cut for each section did not exceed 2.7 m. Microscopic analysis of the cutting edges revealed that significant changes in the cutting edge radii r_β occurred during the initial cuts, which corresponded to a cutting length of $l_m = 300$ mm in these experiments. Beyond this initial phase, the cutting edges remained predominantly stable.

2.3. Material

The tested CFRP panels were fabricated from autoclave-cured prepregs consisting of HexPly 913 epoxy matrix and HTS carbon fibres in a $[0°]_{16}$ layup. The material's thermal conductivity was experimentally measured with an LFA method (LINSEIS XFA600 according to ASTM E 1461:2013) at an ambient temperature of 28 °C and is provided in Table 2, along with other material properties as per [30].

Separate tests were conducted to determine the CFRP infrared emissivity. An external heater was used to establish a steady temperature state in a CFRP panel with installed thermocouples. An emissivity value of $\xi_m = 0.95$ was adopted for the temperature range of 30 °C–140 °C, ensuring that the average temperature error remained below 3 °C. This value corresponds to typical levels reported in the

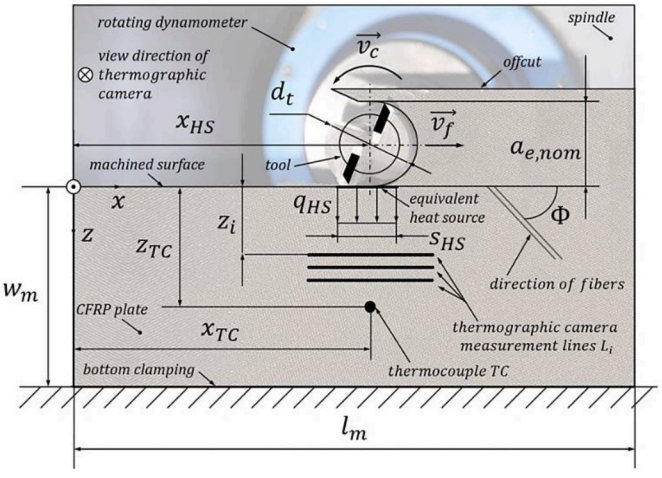

Fig. 1. Schematic representation of machining situation of CFRP-orthotropic panel.

Table 1
Parameters of the experimental setup and the used tools.

Parameter	Symbol	Value	Unit
Length of machined path	l_m	300	mm
Distance in transversal direction from cutting surface to plate clamping	w_m	50	mm
Distances to the lines of measurement with the thermographic camera	z_i	0.7/0.92/1.38	mm
Horizontal distance to TC	x_{TC}	177.8	mm
Vertical distance from machined surface to TC	z_{TC}	1.5	mm
Tool diameter	d_t	12	mm

literature for similar materials [31]. Higher temperatures were not tested to prevent thermal degradation of the plate, as the glass transition temperature of the matrix is 150.1 °C. According to the literature [32], the overall temperature dependence of material emissivity shows a tendency toward lower emissivity values at elevated temperatures. Consequently, at higher temperatures, assuming a constant emissivity value could lead to an underestimation of the actual material temperature when measured by an infrared camera.

2.4. Process parameters and measurement equipment

The same test series were conducted using each of the tools, with the process parameters provided in Table 3. The experiments enable the analysis of the cutting speed's influence by comparing the results from test series TS-I and TS-II, both carried out in full cut. The effect of the combined variation of cutting speed v_c and nominal width of cut $a_{e,nom}$ at a constant material removal rate Q_W can be observed by comparing the results of test series TS-I and TS-III. Additionally, the fibre orientation angle Φ was varied as shown in Table 2. Rectangular CFRP panels were prepared with fibres oriented at corresponding angles Φ to the edge.

Experiments were conducted using a 5-axis machining center Reichenbacher VISION II-Sprint equipped with a 4-component rotational dynamometer Kistler 9170A and a signal conditioner Kistler 5238B for measuring torque M_z. The measurement accuracy was 0.1 Nm. The torque value M_z was essential for calculating the corresponding cutting power:

$$P_c = 2\pi \cdot M_z \cdot n_z = 2 \cdot M_z \cdot \frac{v_c}{d_t}, \quad (1)$$

where n_z is the number of revolutions. The use of the rotating dynamometer allowed for the analysis of the actual cutting power used in the material's mechanical processing, as opposed to the machining center spindle power, which includes transmission losses.

The experimental setup included shielded type J thermocouples (Fe/CuNi) from TC Direct and a frontally positioned thermographic camera Micro-Epsilon ThermoIMAGER TIM VGA 640 x 480 px, 32 Hz, noise equivalent temperature difference NETD 40 mK, for measuring the temperature of the CFRP panel in the vicinity of the tool. The hot junction of the thermocouple was placed in the workpiece in a hole with a diameter of 0.6 mm and a depth of 2 mm, filled with thermal conducting paste.

Extensive testing showed that best possibilities for modeling are provided by using a combined set of measurement data. This set includes both temperatures measured by the thermographic camera at small distances z_i from the machined surface, as well as temperatures measured by the thermocouple at a minimal safe distance z_{TC} (see Table 1). At this distance the installation of measuring gauges posed no risk of mechanical damage to the equipment.

The temperatures measured by the thermographic camera were cross-checked with the thermocouple measurements. The deviation

Table 2
Material properties of CFRP workpiece.

Parameter	Symbol	Value	Unit
Thermal conductivity in 1st orthotropy direction (parallel to fibres)	k_{11}	7.695	$W \cdot m^{-1} \cdot K^{-1}$
Thermal conductivity in 2nd orthotropy direction (perpendicular to fibres)	k_{33}	0.630	$W \cdot m^{-1} \cdot K^{-1}$
Specific heat capacity	c_p	879	$J \cdot kg^{-1} \cdot K^{-1}$
Density	ρ_w	1516	$kg \cdot m^{-3}$
Fibre volume content	ϑ_{FVC}	52	%
Glass transition temperature	T_g	150.1	°C
Matrix decomposition temperature	T_d	407.2	°C
Temperature emissivity	ξ_m	0.95	–
Panel thickness (equal to the depth of cut)	a_p	4.72	mm
Fibre orientation angle	Φ	45/90/135	°

Table 3
Investigated range of machining parameters.

Parameter	Symbol	Values in test series (TS)			Unit
Test series number		TS-I	TS-II	TS-III	
Cutting speed	v_c	100	450	450	$\frac{m}{min}$
Feed	f	0.06	0.06	0.107	mm
Feed rate	v_f	0.159	0.716	1.273	$\frac{m}{min}$
Nominal width of cut	$a_{e,nom}$	12	12	1.5	mm
Material removal rate	Q_W	9.55	42.97	9.55	$\frac{cm^3}{min}$

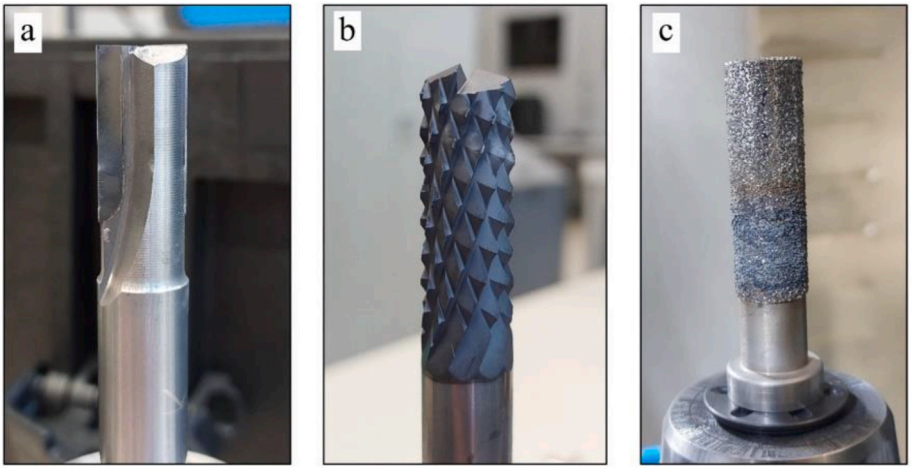

Fig. 2. Tested peripheral milling tools: double-edged PCD cutter (a) and router (b) of defined geometry, grinding pin (c).

between the temperature values obtained from both methods did not exceed 4 °C or 3 % of the measured value, which is within the accuracy range of the devices used.

Chips produced during milling were removed using a Schuko vacuuming system with a suction capacity of 13,600 m^3/h. This minimized the impact of chips resting on the workpiece and affecting its temperature.

2.5. Analytical modeling

The temperatures measured by the thermographic camera and thermocouples were used to fit the analytical model of the temperature field in the workpiece for machining of orthotropic material with arbitrary orthotropy direction [1]:

$$\Delta T(x_n, z_n) = \frac{q_{HS}}{\pi\sqrt{k_{11}k_{33}}} \cdot \int_{x_n - s_{HS}/2}^{x_n + s_{HS}/2} \exp\left(\frac{\rho_w C_p v_f}{2k_{11}k_{33}} \cdot \left[(k_{11} - k_{33})\left((x_n - x_{HS}) \cdot \cos^2\Phi + z_n \cdot \sin\Phi \cdot \cos\Phi\right) - k_{11} \cdot (x_n - x_{HS})\right]\right) \cdot K_0 \left\{\frac{\rho_w C_p v_f}{2k_{11}k_{33}} \cdot \left(k_{11} - (k_{11} - k_{33})\right.\right.$$
$$\left.\left. \cdot \cos^2\Phi\right)^{1/2}\left[(k_{11} - k_{33}) \cdot \left(\left(z_n^2 - (x_n - x_{HS})^2\right) \cdot \cos^2\Phi - 2z_n \cdot (x_n - x_{HS}) \cdot \sin\Phi \cdot \cos\Phi\right) + k_{11} \cdot (x_n - x_{HS})^2 + k_{33} \cdot z_n^2\right]^{1/2}\right\} d(x_n - x_{HS}), \quad (2)$$

where the main orthotropy direction coincides with the fibre reinforcement direction and is therefore defined by the fibre orientation angle Φ. K_0 is the modified Bessel function of the second kind of order zero. Other symbols correspond to those mentioned previously. The temperature field change along the *y* direction is not considered.

Thus, the region of tool-material interaction is modeled as a moving strip heat source in a steady state according to Eq. (2). The heat source is characterized by its shape, which is a rectangle moving along the machined surface with a width equal to the panel thickness a_p and a variable length s_{HS}, as well as its intensity, represented by the equivalent heat flux q_{HS}, as shown in Fig. 1. The differences in the physical cutting processes associated with the three tested tool types manifest as variations in the thermal parameters of the moving heat source, namely s_{HS} and q_{HS}. This allows for a clear and descriptive comparison of the thermal aspects of tool-material interaction when using different tools, as well as under varying machining conditions, as listed in Table 3. The equivalent heat flux q_{HS} and the thermal contact length s_{HS} of the moving strip heat source are related as follows:

$$s_{HS} = P_{HS} / \left(q_{HS} \cdot a_p\right), \quad (3)$$

where P_{HS} is a heat flow from the moving strip heat source into the workpiece. The proportion of mechanical processing power P_c that is converted into heating of the machined surface was determined using the ratio of heat flow to cutting power:

$$R_W = \frac{P_{HS}}{P_c}. \quad (4)$$

The values of the heat flow P_{HS}, the equivalent heat flux q_{HS} and the thermal contact length s_{HS} were determined using the Trust-Region-Reflective Least Squares Algorithm, as described in Ref. [1]. This was done by solving the nonlinear least-squares problem to fit the model in Eq. (2) to the experimental average maximum temperature changes $\Delta T_{max}(z_n)$ measured by the thermographic camera $\Delta T_{max}(z_n = z_i)$ and the thermocouples $\Delta T_{max}(z_n = z_{TC})$ at various distances from the machined surface as indicated above.

3. Results and discussion

The experiments resulted in a set of measured temperatures $\Delta T_{max,exp}$ and torques M_z obtained during the processing of CFRP panels with the three tested tools: the two-tooth PCD cutter, the router, and the grinding pin. The measured temperature values $\Delta T_{max,exp}$ were used to determine the equivalent heat flux q_{HS} and the thermal contact length s_{HS} according to Eq. (2), as described in the previous section.

These values enabled the simulation of temperature fields in the vicinity of the machined surface and the maximum temperature changes ΔT_{max} at the machined surface using Eq. (2). The heat flow from the moving heat source into the workpiece P_{HS} was calculated using Eq. (3). Subsequently, the heat flow ratio R_W was calculated according to Eqs. (1) and (4).

3.1. Tool influence on the dependency of the temperature changes ΔT_{max} on the fibre orientation angle Φ

Simulated values of the maximum temperature changes ΔT_{max} at the machined surface across all test series and fibre orientation angles Φ indicate that the glass transition temperature of the matrix $T_g = 150.1$ °C was exceeded in most experiments for all the tested tools (Fig. 3). In many cases, the matrix decomposition temperature T_d was reached. In these cases, matrix decomposition occurs very close to the machined surface, which is not covered by the model.

To verify the model's adequacy, the maximum temperature change ΔT_{max} was simulated at a distance of $z = 0.7$ mm from the machined surface, where the temperature was also experimentally measured using the thermographic camera. The mean deviation between the simulated ΔT_{max} and the measured $\Delta T_{max,exp}$ maximum temperature changes at this distance from the machined surface was 3.1 °C, indicating that the simulation results are in close agreement with the experimental values.

The highest simulated temperature changes ΔT_{max} at the machined surface were obtained for all the tested tools at the fibre orientation angle $\Phi = 135°$. Nevertheless, the test series in which this is observed, as well as the patterns relative to other test cases, differ among the tools. The maximum simulated ΔT_{max} occurred for the cutter in TS-III at the higher cutting speed and lower width of cut, $\Delta T_{max} = 445.6$ °C, for the router in TS-II at the higher cutting speed and higher width of cut, $\Delta T_{max} = 772$ °C, and for the grinding pin in TS-I at the lower cutting speed and higher width of cut, $\Delta T_{max} = 714.1$ °C.

Because tools commonly used in practice were studied, finding out the differences between the tool types was of primary interest. Quantitative comparisons are only possible to a limited extent for the two tool types with defined cutting-edge geometry. In addition, fundamental differences in performance of the tool types with defined and undefined cutting-edge geometry become clear from the obtained results. Due to the higher number of cutting edges of the router compared to the cutter and the associated lower chip thicknesses *h*, the material is removed in significantly more and smaller particles. This leads to in most cases higher temperature changes ΔT_{max} for the router compared to the cutter. On the other hand, it explains that in case of the cutter with higher chip thicknesses *h*, large-scale break-outs of material particles are frequently observed, that will be described in Section 3.3.

Comparing the temperature changes ΔT_{max} between the tools of defined geometry and the grinding pin, the patterns of temperature changes ΔT_{max} differ significantly.

The minimum simulated ΔT_{max} occurred for the cutter in TS-I at $\Phi = 90°$, $\Delta T_{max} = 117.1$ °C, for the router in TS-I at $\Phi = 90°$, $\Delta T_{max} =$

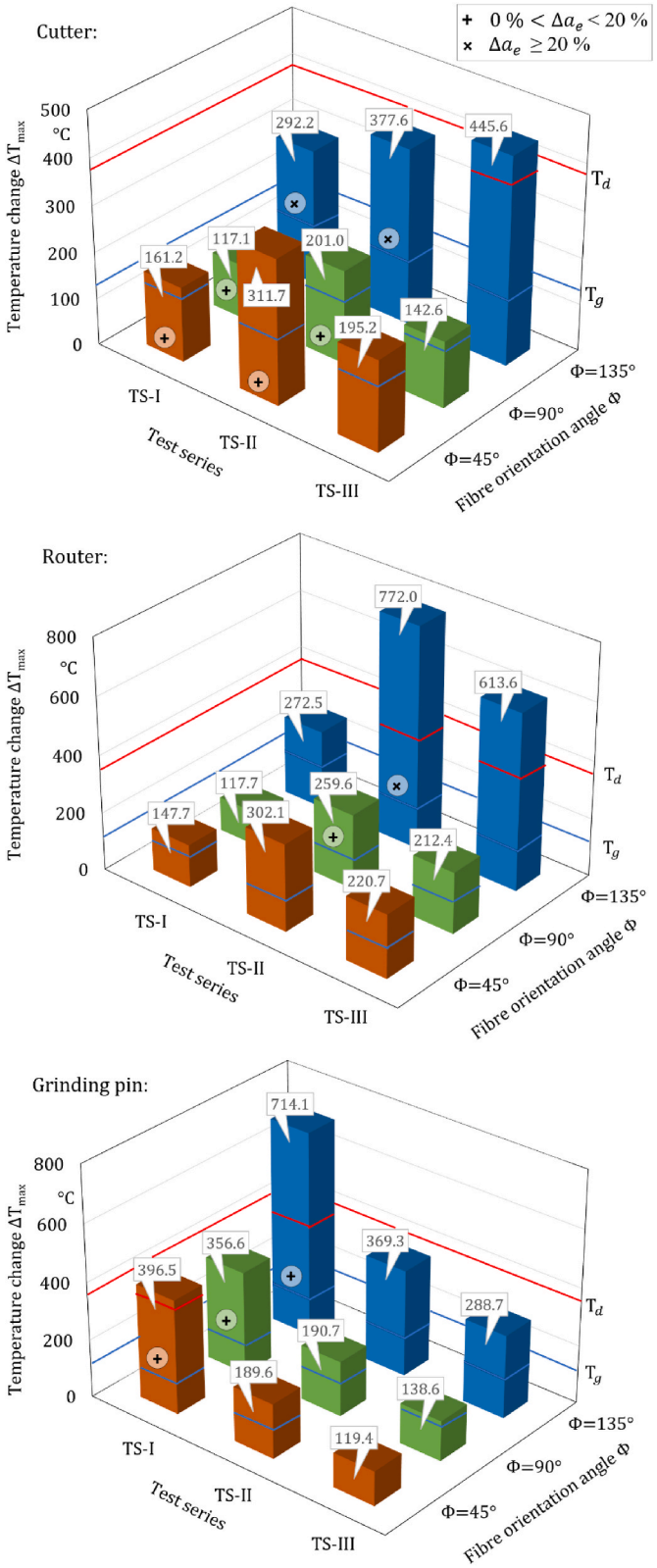

Fig. 3. Simulated maximum temperature changes at the machined surface ΔT_{max} depending on the tool type, tested parameter series TS-I, II, III according to Table 3 and fibre orientation angles Φ, whereas relative change in the width of cut Δa_e is given as described in Section 3.3.

117.7 °C, and for the grinding pin in TS-III at $\Phi = 45°$, $\Delta T_{max} = 119.4$ °C. Therefore, minimum values of ΔT_{max} were found for the fibre orientation angle $\Phi = 90°$ for the cutter and the router, and had similar values for $\Phi = 45°$ and $\Phi = 90°$ for the grinding pin. The relation on the fibre orientation angle for all the tools can be attributed to the high thermal conductivity k_{11} along the fibre direction, which facilitates more efficient heat transfer from the contact zone perpendicular to the machined surface in the case of $\Phi = 90°$. The differences between the tools in dependency patterns for $\Phi = 45°$ and $\Phi = 90°$ can be referred to the higher number of pulsed point contacts and according heat accumulation of the router compared to the pulsed linear contact of the cutter. It has to be pointed out that the temperature changes do not correlate to the measured cutting power, as described in Section 3.4. Only local effects close to the machined surface determine the temperature changes ΔT_{max}, but not the machining processes at the entire range of engagement angles φ, which determine the cutting power. As a consequence, large-scale break-outs of material particles are also of minor importance for the temperature changes ΔT_{max} of the machined surface.

The obtained data confirm the findings in Ref. [19], which indicate that temperatures in abrasive circular cutting do not exceed those in end milling at similar feed rates and material thickness. This can be explained by the continuous surface contact corresponding to the high number of abrasive grains simultaneously in contact with the workpiece, facilitating heat transfer from the contact zone into the tool. This corresponds to the higher thermal contact length s_{HS} of the grinding pin compared to the other tools, as discussed below in Section 3.3.

The results for the fibre orientation angles $\Phi = 45°$ and $\Phi = 135°$ (Fig. 3) align with the observations in Ref. [33] as follows. In up-cut milling, the initial tool path close to the machined surface significantly influences the temperatures reached there. For $\Phi = 135°$, this corresponds to the engagement angles $\varphi = 0° \ldots 22.5°$ (so that $a_e < 0.5$ mm) and the corresponding fibre cutting angles $\theta = 135° \ldots 157.5°$. According to Ref. [33], this range of θ is associated with higher friction coefficients under similar processing parameters v_c, f, a_e. In contrast, for $\Phi = 45°$, the initial tool path occurs at $\theta = 45° \ldots 67.5°$, which, as per [33], corresponds to minimal friction coefficients. Consequently, the instantaneous friction forces close to the machined surface are expected to be higher for the fibre orientation angle $\Phi = 135°$ than for $\Phi = 45°$. Higher friction forces result in greater mechanical energy dissipation as heat, leading to more significant local temperature changes ΔT_{max} at the machined surface. This conclusion is corroborated by the current test results for all the tested tools (Fig. 3).

3.2. Tool influence on the dependency of the temperature changes ΔT_{max} on the process parameters

Highest simulated temperature changes ΔT_{max} at the machined surface for the tested tools of defined geometry, namely the cutter and the router, were predominantly obtained in TS-II (Fig. 3), that corresponds to nominal full cut at the higher cutting speed $v_c = 450$ m/min, as listed in Table 3. These results align with expectations when compared to TS-I, which corresponds to the lower cutting speed of $v_c = 100$ m/min and a correspondingly lower material removal rate Q_W. The cutting power P_c, as shown later, is also higher for TS-II.

The resulting temperature changes ΔT_{max} for a constant material removal rate Q_w but at different v_c- f- $a_{e,nom}$ combinations are compared based on TS-I and TS-III. For the cutter and the router, ΔT_{max} is higher in partial cut at the higher cutting speed $v_c = 450$ m/min (TS-III) than in full cut at the lower cutting speed $v_c = 100$ m/min (TS-I).

The longer cooling path of the cutting edges and the correspondingly shorter time during which the cutting edge is in engagement in partial cut (TS-III) compared to full cut (TS-I) appear to have a minor influence on temperature changes. Instead, the increased cutting speed v_c plays a dominant role. These results suggest that the concept of high-speed machining in contour milling of CFRP does not offer obvious advantages from a thermal point of view.

The temperature differences are more pronounced for the multi-tooth router made of diamond-coated tungsten carbide compared to the two-tooth cutter with PCD blanks. This distinction can be attributed to the following factors. At the lower cutting speed, the higher number of cutting edges of the multi-tooth router in engagement results in slightly reduced temperature changes compared to the two-tooth cutter. At the higher cutting speed, the significantly greater thermal conductivity of the PCD-equipped two-tooth cutter, compared to the diamond-coated tungsten carbide router, leads to substantially lower temperature changes.

In contrast, the abrasive tool demonstrates a completely different pattern of temperature changes dependency on process parameter combinations compared to the tools of defined cutting-edge geometry. This behavior is explained with several factors. The negative rake angles γ_f of cutting edges of abrasive tool grains as well as their absent clearance angles α_f and extremely high cutting-edge radii r_β significantly contribute to heat generation due to crushing workpiece material particles. This process involves forming multiple splitting surfaces, as compared to the cutting action of tools of defined edges. The abrasive tool removes material locally and has a continuous surface contact which is much larger compared to the tools of defined cutting edges, which are characterized with pulsed linear and pulsed point surface contact.

The highest simulated temperature change ΔT_{max} at the machined surface for the abrasive tool was observed at the lower cutting speed v_c = 100 m/min (TS-I). At this speed, the cutter and the router exhibit minimal temperature changes. Thus, the much larger continuous surface contact zone of the grinding pin seems to be detrimental at the lower cutting speed as more heat is transferred into the workpiece surface by the high number of grains under conditions of prolonged contact time.

Interestingly, in partial cut (TS-III), the grinding pin exhibits lower maximum temperature changes ΔT_{max} than the cutters of defined cutting-edge geometry, despite the cutting power P_c is of similar magnitude (see Section 3.4, Fig. 5). Under these cutting conditions of high cutting speed v_c and low width of cut $a_{e,nom}$, the heat capacity of the abrasive grains combined with their longer cooling path compared to the engagement path enables favorable heat dissipation from the cutting zone and further air cooling of the grinding pin for all the fibre orientation angles Φ.

In addition, in accordance with the findings in Ref. [19], it can be concluded that in edge trimming with disc-like diamond grinding wheels, favorable low workpiece temperatures can be ensured as the cutting conditions are similar.

An in-depth analysis of the shape and extension of the temperature fields depending on the tool type in combination with the velocity v_f of the moving heat source is necessary to even better understand the contrasting temperature results observed between the tools of defined geometry and the grinding pin. With regard to the detailed engagement conditions in the cutting zone, grinding is characterized by quasi-continuous heat exchange from numerous grains in continuous surface contact with the workpiece, while cutting with defined cutting edges involves pulsed heat exchange, as individual cutting edges intermittently engage and disengage with the material.

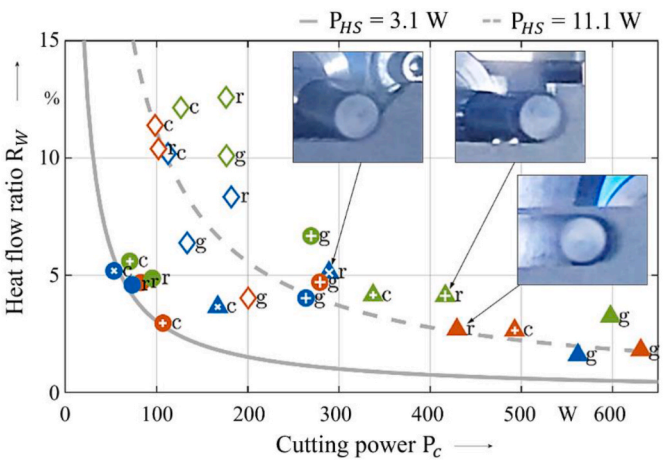

Fig. 5. The heat flow ratio R_W vs. the cutting power P_c at varying cutting speeds v_c, feeds f, nominal widths of cut $a_{e,nom}$ and fibre orientation angles Φ for the three tested tools. Legend as in Fig. 4.

3.3. Tool influence on the heat source parameters q_{HS} and s_{HS}

Fig. 4 presents the modeled values of the equivalent heat flux q_{HS} and the thermal contact length s_{HS}, along with fitting curves based on Eq. (3). Each curve corresponds to a specific value of the heat flow P_{HS}, as indicated in the legend.

The values of the thermal contact length s_{HS} cluster into two distinct regions depending on the fibre orientation angles Φ. At Φ = 90°, the trimming processes are characterized with higher s_{HS} in the range of 2.5 mm < s_{HS} < 7 mm. At Φ = 45° and Φ = 135°, lower s_{HS} values are found, 0.5 mm < s_{HS} < 3 mm. This observation aligns with the previously noted lower simulated temperature changes ΔT_{max} at Φ = 90°. Therefore, the better heat conduction in the direction of the reinforcement fibres, which are perpendicular to the machined surface at Φ = 90°, relates to the higher modeled thermal contact length s_{HS} for all the tested tools

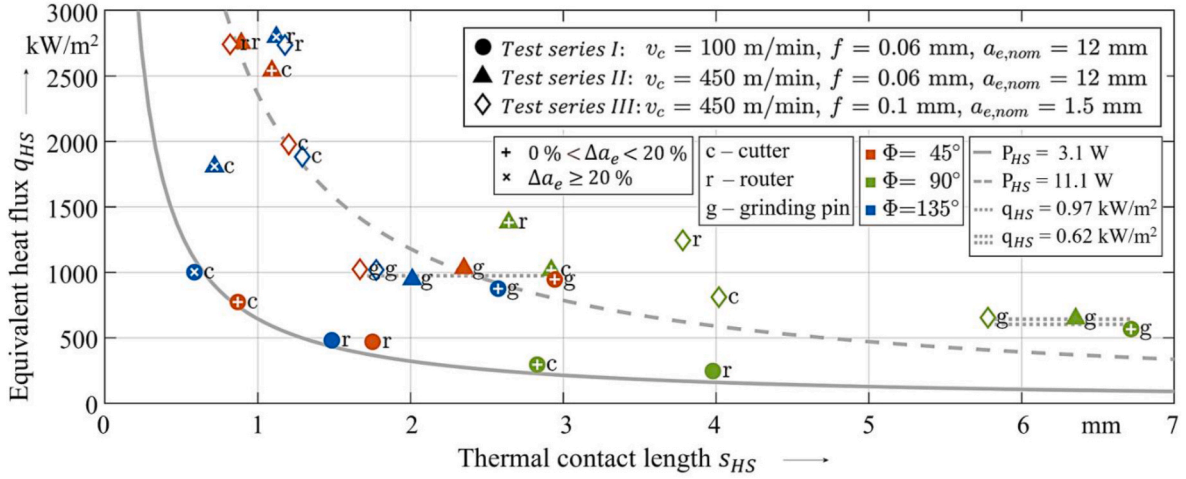

Fig. 4. Equivalent heat flux q_{HS} vs. thermal contact length s_{HS} at varying cutting speed v_c, feed f, nominal width of cut $a_{e,nom}$ and fibre orientation angle Φ

regardless of type.

The maximal difference in s_{HS} between the fibre orientation angles $\Phi = 45°$ and $\Phi = 135°$ did not exceed 0.5 mm for all the tools under the same conditions. For both Φ, the inclination of the main orthotropy direction, for which the thermal conductivity k_{11} for the tested UD-CFRP material is much higher than k_{33}, plays a primary role in defining s_{HS} for all the tools and may be characterized by the fibre orientation symmetry angle $\zeta_\Phi = |\Phi - 90°| = 45°$, as recently shown in Ref. [21].

For each tested Φ for the nominal full cut in test series TS-I, s_{HS} for the grinding pin is from 2 to 4 times higher than for the cutter and approximately 1.7 times higher than for the router. At the higher cutting speed in test series TS-II and TS-III, s_{HS} for the router and the cutter are closer to each other than at the lower v_c in TS-I. In TS-II, s_{HS} for the router and the cutter are approximately 2.3 times, and in test series TS-III 1.5 times smaller than for the grinding pin. In all cases the grinding pin exhibits the highest s_{HS} values compared to the other tools for each tested Φ. Thus, the more cutting edges are in engagement, the higher s_{HS}.

For each tested Φ, the grinding pin has lower s_{HS} values in TS-III compared to TS-II, with the highest values observed in TS-I. For the router, s_{HS} in TS-I is also slightly higher than in both TS-II and TS-III, just as for the grinding pin. But for the cutter s_{HS} already tends to be lowest in TS-I for each tested Φ. Thus, different cutting conditions affect the contact length s_{HS} for the investigated tool types in a completely different way.

It should be noticed that break-outs of material particles occur in some cutting tests. They were observed primarily with the PCD cutter and least of all with the grinding pin. This can be explained by the much higher engagement impacts in the case of the continuous cutting edges and chip thickness h of the PCD cutter, compared to the significantly lower engagement impacts and chip thicknesses h of the router and, in particular, the grinding pin, due to the number and form of the point-shaped cutting edges. The break-outs result in a smaller effective width of cut $a_{e,eff}$. The relative change in the width of cut $\Delta a_e = (a_{e,nom} - a_{e,eff})/a_{e,nom}$ was classified and is indicated in Figs. 3–5. For the PCD cutter, higher Δa_e relate to minimal values of s_{HS} according to simulations.

The equivalent heat flux q_{HS} demonstrates a higher dependency on the cutting speed v_c for both the cutter and the router, while the heat flow P_{HS} remains predominantly stable for each v_c. The fitting curves in Fig. 4 according to Eq. (3) indicate similar P_{HS} close to 3 W for the cutter and the router for all Φ in TS-I at the lower $v_c = 100$ m/min. In test series TS-II and TS-III at $v_c = 450$ m/min, an average P_{HS} is close to 11 W for both tools of defined geometry. Surprisingly, the 4-times higher material removal rate Q_W does not lead to a considerable increase in P_{HS} from test series TS-III to TS-II. This means that the heat exchange occurs predominantly in the vicinity of the machined surface and is only to a minor extent affected by the effective width of cut $a_{e,eff}$.

For each separately considered Φ in test series TS-II and TS-III at the higher $v_c = 450$ m/min, the equivalent heat flux q_{HS} demonstrates higher values for the router than for the cutter, with the mean difference of 602 k W·m^{-2} significantly greater than zero ($p = 0.005$). In contrast, in TS-I at the lower $v_c = 100$ m/min the equivalent heat flux q_{HS} for the router is slightly lower than for the cutter. That fully correlates with the previously discussed pattern for the differences in the simulated maximum temperature changes ΔT_{max} for different test series (Section 3.2, Fig. 3).

According to Eq. (2), ΔT_{max} is influenced by several parameters, which take different values across the realized test series. These parameters are s_{HS}, q_{HS} and v_f. A higher v_f, as in TS-III compared to TS-II, leads to a lower heat accumulation per unit length of cut and therefore to mostly lower ΔT_{max} even at the same P_{HS}. For the tools of defined geometry also the heat flux q_{HS} exerts an influence on the resulting temperature, as it can be seen from Fig. 4. Fig. 4 shows that for this case q_{HS} is mostly lower in TS-III compared to TS-II. This indicates that the influence of the speed rate v_f in simulations according to Eq. (3) is not sufficient to fully explain the experimental values of the temperature changes ΔT_{max}. This helps to distinguish the influence of the feed rate v_f as the velocity of the moving heat source from the other factors affecting the temperature increase at the machined surface, whose influence is therefore expressed with q_{HS}. Among them is for instance the effective width of cut $a_{e,eff}$ representing the path of the tool engagement. In the future the model might be extended to introduce the heat source moving along subsequent cutting paths instead of the simplified heat source moving along the length of the machined surface.

In contrast to that, in the case of the continuous engagement of the cutting edges with the workpiece, as provided by the grinding pin, the values of the heat flow P_{HS} are spread across a wider range but the equivalent heat flux remains close to a constant value of $q_{HS} = 974$ k W·m^{-2} for the fibre orientation symmetry angle $\zeta_\Phi = 45°$ and to $q_{HS} = 624$ k W·m^{-2} for $\zeta_\Phi = 0°$. The resulting heat flow P_{HS} is achieved due to differentiated thermal contact lengths s_{HS}, which are highest at $v_c = 100$ m/min in TS-I and lowest in partial cut in TS-III, for each separately considered fibre orientation angle Φ.

Both tools of defined geometry exhibit similar trends in the thermal parameters of the machining process. At the higher v_c, the router shows higher q_{HS} than the cutter, and vice versa. s_{HS} is, on average, twice as high for the router than for the cutter at the lower v_c. This may indicate the model's sensitivity to the fact that heat is liberated simultaneously at several teeth of the router, compared to the concentrated tooth-material interaction region of single teeth being in engagement in the case of the cutter.

For all the tools for the fibre orientation symmetry angle $\zeta_\Phi = 45°$ (i.e. for $\Phi = 45°$ and $\Phi = 135°$), the equivalent heat flux q_{HS} is greater than for $\zeta_\Phi = 0°$ (i.e. for $\Phi = 90°$).

3.4. Tool influence on the ratio R_W of heat flow P_{HS} to cutting power P_c

The relationships between cutting power P_c and heat flow P_{HS} are shown in Fig. 5. The highest cutting power P_c for all the tools is observed for the case of full cut at the higher cutting speed v_c, i.e., in TS-II. The grinding pin is characterized by higher P_c than the tools of defined geometry in full cut at both tested cutting speeds v_c, i.e., in both TS-I and TS-II. In TS-I, P_c for the grinding pin is three times higher. Both cutting tools of defined cutting edges geometry and the grinding pin show similar P_c in partial cut at the higher cutting speed, i.e., in TS-III. The minimum P_c values are observed for the tools of defined geometry in full cut at the lower cutting speed v_c in test series TS-I. P_c in TS-III is higher than in TS-I for the tools of defined geometry, but lower for the grinding pin.

Only in full cut, i.e., in TS-I and TS-II, considerable material break-outs occur under the cutting conditions marked in Fig. 5, which significantly reduce the cutting power P_c, compared to the undisturbed process. Exemplary in-process photos for disturbed and undisturbed processes are shown in Fig. 5. When comparing Δa_e values less than 20 % to those greater than 20 %, the drop in P_c is higher for higher Δa_e, as expected.

Regarding the influence of the fibre orientation on cutting power P_c, the cutting power mostly decreases with increasing fibre orientation angle from $\Phi = 45°$ to $\Phi = 135°$. For $\Phi = 90°$, P_c usually takes intermediate values, compared to the other tested Φ. This holds for all the tools in full cut and for the grinding pin in partial cut.

In full cut, P_c is mainly influenced by the cutting action in the range of engagement angles $\varphi \approx 90°$, where the maximum chip thickness h occurs. This is particularly relevant for the tools of defined geometry, which are characterized by significantly higher chip thickness h per tooth. The range of $\varphi \approx 90°$ corresponds to a range of fibre cutting angles θ, shifted with respect to the fibre orientation angle Φ by approximately 90°. This results in $\theta = 135°$ in the region of the highest chip thicknesses h when $\Phi = 45°$. It is well known that the highest cutting forces occur near $\theta = 135°$ [20,34]. In partial cut, the influence of the fibre

orientation angle on the cutting power generated by the grinding pin and the tools of defined geometry is controversial, which cannot be sufficiently explained so far.

With respect to the influence of alternative full cut versus partial cut at a constant material removal rate Q_W (TS-I vs. TS-III) on cutting power P_c, no clear trend is observed. That means that high-speed cutting strategies, well-known in metal cutting, are not applicable to CFRP machining.

Regarding the heat flow ratio R_W, similar R_W are found in test series TS-I and TS-II, which result in much higher actual heat flows P_{HS}, see Eq. (4), due to the much higher P_c in TS-II, that is expected as a result of the higher cutting speed v_c. The higher actual heat flow P_{HS} results in a higher thermal loading of the CFRP-plates in the cutting zone.

Although R_W is relatively low in the experiments with the grinding pin in TS-I, high temperatures at the machined surface are still observed due to the high P_c and the prolonged time of interaction with the tool per unit length of cut (see Fig. 3).

The highest heat flow ratios R_W are observed in partial cut in TS-III, especially for the tools of defined geometry. The heat flow ratios R_W in full cut (TS-I and TS-II) are approximately half as low. In TS-II, the R_W values tend to be slightly lower than in TS-I for all the tools, particularly for the grinding pin. Therefore, the lowest R_W values are observed for the grinding pin in full cut at the higher cutting speed v_c, i.e., in TS-II.

In TS-II and TS-III, i.e., in test series at higher cutting speed v_c, the R_W values are higher for the tools of defined geometry than for the grinding pin at each respective Φ. This, along with approximately similar cutting power, results in lower heat flows R_W and maximum temperature changes ΔT_{max} for the grinding pin in partial cut (TS-III). This is consistent with Fig. 3 and can be explained by the favorable heat transfer into the numerous grains of the grinding pin. Therefore, the grinding pin in partial cut exerts a lower thermal load on the CFRP panel compared to the tools of defined geometry.

At the lower cutting speed v_c in TS-I all the tools are characterized with similar R_W, meaning a similar percentage of the power is converted into heat flow P_{HS} relative to the cutting power P_c despite the different levels of P_c for the tools of defined geometry and the grinding pin.

The heat flow ratio R_W at the fibre orientation angle $\Phi = 90°$ is generally higher than at $\Phi = 45°$ and $\Phi = 135°$ for all the tools. This may be due to the maximum thermal conductivity along the fibre direction at $\Phi = 90°$.

Cutting conditions that result in a constant heat flow P_{HS} are represented by hyperbolas in Fig. 5 according to Eq. (4). At the lower cutting speed v_c in TS-I, the heat flow P_{HS} is low and nearly constant for the tools of defined geometry. In contrast, the heat flow P_{HS} is more than three times higher for the grinding pin in TS-I. At the higher cutting speed v_c in TS-II and TS-III, no dependencies of P_{HS} on the tool type and full vs. partial cut are observed. This suggests that, with regard to the thermal load on the boundary zone of the workpiece, finishing offers no advantages over roughing.

In Fig. 5, it can be seen that the heat flow P_{HS} is generally highest for the fibre orientation angle $\Phi = 90°$ in all test series for all the tools, which corresponds to the fibre orientation symmetry angle $\zeta_\Phi = 0°$. This may be explained by the good heat conduction normal to the machined surface.

The influence of the alternative full cut versus partial cut at a constant material removal rate Q_W (TS-I vs. TS-III) on the heat flow P_{HS} aligns with the influence on the cutting power P_c as discussed above.

4. Summary and outlook

The thermal performance of a PCD cutter, router and grinding pin was investigated in upcut milling of UD-CFRP, based on experiments and simulations using an analytical model. For the first time by means of the utilized model, the influence of different tool types on the thermal parameters contact length s_{HS} and equivalent heat flux q_{HS} was systematically identified, thus providing a comparison of the tool types and allowing for the identification of both common and distinct patterns in the CFRP thermal response in machining. The findings can be summarized as follows.

- All the tools are characterized by high simulated temperatures at the machined surface, which exceed the glass transition temperature T_g of the CFRP matrix under most of the tested cutting conditions. Simulated and measured maximum temperature changes ΔT_{max} close to the machined surface agree well with a mean deviation of 3.1 °C.
- The simulated maximum temperature changes ΔT_{max} at the machined surface are determined by the heat flow P_{HS} (which accounts for the influence of the equivalent heat flux q_{HS} and the thermal contact length s_{HS}), and the heat source speed, which is equal the feed rate v_f (depending on v_c and f), of the tool.
- For the tools of defined geometry with a non-continuous engagement of the cutting edges, namely for the cutter and the router, the heat flow P_{HS} demonstrates considerably higher values at the higher cutting speed v_c. For the abrasive tool with a continuous engagement, namely for the grinding pin, P_{HS} does not demonstrate any clear dependency on v_c.
- For all tested tools, the equivalent heat flux q_{HS} clearly tends to lower and the thermal contact length s_{HS} to higher values at the fibre orientation angle $\Phi = 90°$ and the fibre orientation symmetry angle $\zeta_\Phi = 0°$ at the same other conditions, and demonstrate the opposite tendency at $\Phi = 45°$ and $\Phi = 135°$, i.e. at $\zeta_\Phi = 45°$.
- For the cutter and the router, minimum values of q_{HS} and maximum values of s_{HS} and P_{HS} correspond to minimum ΔT_{max} at $\Phi = 90°$ and $\zeta_\Phi = 0°$ due to favorable heat conduction at this fibre orientation angle.
- For the cutter and the router, q_{HS} and P_{HS} demonstrate considerably lower values at the lower cutting speed of $v_c = 100$ m/min at same other conditions, compared to $v_c = 450$ m/min. Moreover, ΔT_{max} is significantly higher for the higher v_c at same fibre orientation angles irrespective of nominal width of cut, feed rate, and material removal rate. Hence, high-speed machining in contour milling of CFRP does not offer obvious advantages from a thermal point of view.
- For the grinding pin, q_{HS} assumes constant values as a function of ζ_Φ, regardless of the other process parameters. Apart from the described dependency on ζ_Φ, s_{HS} demonstrates higher values for lower cutting speed v_c regardless of the other process parameters, as well. Moreover, s_{HS} is reduced for lower $a_{e,nom}$ in partial cut, compared to full cut, due to the reduced geometrical contact length. Thus, the thermal contact length s_{HS} predominantly effects the heat flow P_{HS} and the maximum temperature change ΔT_{max} in grinding. In contrast to the tools of defined cutting edge, ΔT_{max} is lower at the higher cutting speed v_c and lower nominal width of cut.
- Notably, the maximum temperature change ΔT_{max} in grinding at the higher cutting speed v_c in full cut is at a similar level to ΔT_{max} when cutting with defined cutting edges and even lower with the higher v_c in partial cut.
- The tool type-dependent thermal parameters and patterns of their dependencies on the machining conditions are differentiated by the model and can be explained by pulsed point, pulsed linear or continuous surface contact of individual cutting edges.

In the future, the influence of dynamic heating of the individual cutting edges during the cutting path should be investigated, heat flow into the unmachined cut-off material as well as potential use of coolant and radiation and convection effects should be considered.

CRediT authorship contribution statement

Wolfgang Hintze: Writing – review & editing, Writing – original draft, Validation, Supervision, Project administration, Methodology, Investigation, Funding acquisition, Conceptualization. **Ganna**

Shchegel: Writing – original draft, Visualization, Validation, Software, Investigation, Formal analysis, Data curation. **Jan Mehnen:** Software, Methodology, Funding acquisition, Conceptualization. **Carsten Möller:** Writing – review & editing, Supervision, Resources, Project administration, Funding acquisition, Data curation. **Jan Dege:** Writing – review & editing, Validation, Supervision, Project administration.

Declaration of competing interest

The authors declare that they have no known competing financial interests or personal relationships that could have appeared to influence the work reported in this paper.

Acknowledgements

We would like to acknowledge and cordially thank the German Research Foundation DFG for funding support of the project 461768523 GZ: HI 843/14-1 AOBJ: 679098.

Data availability

Data will be made available on request.

References

[1] Mehnen J, Hintze W, Köttner L, Von Wenserski R. Temperature field due to a moving heat source in machining orthotropic composites with arbitrary fiber orientation. Proc CIRP 2019;85:2–7. https://doi.org/10.1016/j.procir.2019.09.019.
[2] Kerrigan K, O'Donnell GE. On the relationship between cutting temperature and workpiece polymer degradation during CFRP edge trimming. Proc CIRP 2016;55:170–5. https://doi.org/10.1016/j.procir.2016.08.041.
[3] Seo J, Kim DC, Park H, Kang YS, Park HW. Advancements and challenges in the carbon fiber-reinforced polymer (CFRP) trimming process. Int J Precis Eng Manuf-Green Tech 2024;11:1341–60. https://doi.org/10.1007/s40684-023-00552-1.
[4] Delahaigue J, Chatelain J-F, Lebrun G. Influence of cutting temperature on the tensile strength of a carbon fiber-reinforced polymer. Fibers 2017;5:46. https://doi.org/10.3390/fib5040046.
[5] Sheikh-Ahmad JY, Almaskari F, Hafeez F. Thermal aspects in machining CFRPs: effect of cutter type and cutting parameters. Int J Adv Manuf Technol 2019;100:2569–82. https://doi.org/10.1007/s00170-018-2881-1.
[6] Castillo-Morales A, Rimpault X, Chatelain J-F, Lebrun G. Temperature study during the edge trimming of carbon fiber-reinforced plastic [0]8/Ti6Al4V Stack Material. J Compos Sci 2021;5:137. https://doi.org/10.3390/jcs5050137.
[7] Wang H, Sun J, Li J, Lu L, Li N. Evaluation of cutting force and cutting temperature in milling carbon fiber-reinforced polymer composites. Int J Adv Manuf Technol 2016;82:1517–25. https://doi.org/10.1007/s00170-015-7479-2.
[8] Devan DJ, Almaskari F, Sheikh-Ahmad J, Hafeez F. A study on tool wear of tungsten carbide cutters in edge trimming of CFRP. J Mech Sci Technol 2022;36:2499–510. https://doi.org/10.1007/s12206-022-0432-z.
[9] Ge J, Fu G, Almeida Jr JHS, Jin Y, Sun D. Thermal effect in CFRP machining: temperature field characteristics, heat generation mechanism and thermal damage management. Comp Struct 2025;356:118845. https://doi.org/10.1016/j.compstruct.2025.118845.
[10] Yashiro T, Ogawa T, Sasahara H. Temperature measurement of cutting tool and machined surface layer in milling of CFRP. Int J Mach Tools Manuf 2013;70:63–9. https://doi.org/10.1016/j.ijmachtools.2013.03.009.
[11] Mullier G, Chatelain JF. Influence of thermal damage on the mechanical strength of trimmed CFRP. Int J Mech Mechatron Eng 2014;9:1559–66. https://doi.org/10.5281/zenodo.1109525.
[12] Prakash R, Krishnaraj V, Tarun GS, Vijayagopal M, Kumar GD. Experimental study on temperature effect and tool wear on edge trimming of carbon fiber reinforced plastics. J Appl Mech Mater 2014;592–594:333–8. https://doi.org/10.4028/www.scientific.net/AMM.592-594.333.
[13] Qian M, Xiao J, Wang G, Huang P, Chen Z, Han G. Evaluation of heat generation using a microscopic cutting model with thermo-mechanical coupling for carbon fiber reinforced polymer composites. J Reinf Plast Compos 2020;39:793–804. https://doi.org/10.1177/0731684420931589.
[14] Helmy MO, El-Hofy H, Sasahara H, El-Hofy MH. Rake angle effects on ultrasonic-assisted edge trimming of multidirectional CFRP laminates. Int J Adv Manuf Technol 2021;115:3467–84. https://doi.org/10.1007/s00170-021-07383-x.
[15] Gao C, Xiao J, Xu J, Ke Y. Factor analysis of machining parameters of fiber-reinforced polymer composites based on finite element simulation with experimental investigation. Int J Adv Manuf Technol 2016;83:1113–25. https://doi.org/10.1007/s00170-015-7592-2.
[16] Brouschkin A, Köttner L, Hintze W, Dege J. Prediction of surface profile in CFRP machining through phenomenological analysis and inverse continuous wavelet transformation. Proc CIRP 2024;123:143–8. https://doi.org/10.1016/j.procir.2024.05.027.
[17] Liu Y, Pan Z, Zhang H, Jing X, Zhou H, Chen Y. Thermal-mechanical coupling in drilling high-performance CFRP: scale-span modeling and experimental validation. Compos Struct 2024;331:117903. https://doi.org/10.1016/j.compstruct.2024.117903.
[18] Geier N, Xu J, Poór DI, Dege JH, Davim JP. A review on advanced cutting tools and technologies for edge trimming of carbon fibre reinforced polymer (CFRP) composites. Compos B Eng 2023;266:111037. https://doi.org/10.1016/j.compositesb.2023.111037.
[19] Hintze W, Klingelhöller C. Analysis and modeling of heat flux into the tool in abrasive circular cutting of unidirectional CFRP. Proc CIRP 2017;66:210–4. https://doi.org/10.1016/j.procir.2017.03.305.
[20] Hintze W. CFK-Bearbeitung: Trenntechnologien für Faserverbundkunststoffe und den hybriden Leichtbau. Berlin Heidelberg: Springer; 2021. https://doi.org/10.1007/978-3-662-63265-9.
[21] Hintze W, Shchegel G, Mehnen J, Möller C, Dege J. Modeling of temperature fields in milling of unidirectionally reinforced CFRP depending on the fibre orientation angle and the effective width of cut. Proc CIRP 2025;131:19–25. https://doi.org/10.1016/j.procir.2024.09.006.
[22] Liu L, Qu D, Wang J, Zhang J, Cao H, Dong X. Thermal-field analytical modeling of machined surface layer in high-speed-dry milling UD-CF/PEEK considering thermal anisotropy and nonlinear thermal conductivity. Compos Appl Sci Manuf 2024;176:107864. https://doi.org/10.1016/j.compositesa.2023.107864.
[23] Jaeger JC. Moving sources of heat and the temperature at sliding contacts. J Proc R Soc N S W 1943;76:203–24. https://doi.org/10.5962/p.360338.
[24] Liu J, Chen G, Ji C, Qin X, Li H, Ren C. An investigation of workpiece temperature variation of helical milling for carbon fiber reinforced plastics (CFRP). Int J Mach Tools Manuf 2014;86:89–103. https://doi.org/10.1016/j.ijmachtools.2014.06.008.
[25] Tönshoff HK, Peters J, Inasaki I, Paul T. Modelling and simulation of grinding processes. CIRP Annals 1992;41:677–88. https://doi.org/10.1016/S0007-8506(07)63254-5.
[26] Möhring H-C, Kushner V, Storchak M, Stehle T. Temperature calculation in cutting zones. CIRP Annals 2018;67:61–4. https://doi.org/10.1016/j.cirp.2018.03.009.
[27] Schieber C, Hettig M, Zaeh MF, Heinzel C. 3D modeling and simulation of thermal effects during profile grinding. Prod Eng 2020;14:655–65. https://doi.org/10.1007/s11740-020-00983-8.
[28] Kryzhanivskyy V, Bushlya V, Gutnichenko O, M'Saoubi R, Ståhl J-E. Heat flux in metal cutting: experiment, model, and comparative analysis. Int J Mach Tools Manuf 2018;134:81–97. https://doi.org/10.1016/j.ijmachtools.2018.07.002.
[29] Mehnen J, Hintze W, Koeppe M. Influence of contour radius and fiber orientation on heat accumulation during machining of unidirectional CFRP. MM Sci J 2021;2021:5085–92. https://doi.org/10.17973/mmsj.2021_11_2021156.
[30] Mehnen JP. Modellgestützte Berechnung der thermischen Belastung bei der Zerspanung von unidirektionalem CFK. Dissertation. TU Hamburg; 2023.
[31] Adibekyan A, Kononogova E, Monte C, Hollandt J. Review of PTB measurements on emissivity, reflectivity and transmissivity of semitransparent fiber-reinforced plastic composites. Int J Thermophys 2019;40. https://doi.org/10.1007/s10765-019-2498-0.
[32] Bentz DP. Fire resistive materials: thermal barriers between fires and structures. Thermal conductivity 30/thermal expansion 18. NIST; 2010. p. 1–12. https://tsapps.nist.gov/publication/get_pdf.cfm?pub_id=902567.
[33] Voss R, Seeholzer L, Kuster F, Wegener K. Cutting process tribometer experiments for evaluation of friction coefficient close to a CFRP machining operation. Proc CIRP 2017;66:204–9. https://doi.org/10.1016/j.procir.2017.03.225.
[34] Karpat Y, Bahtiyar O, Değer B. Mechanistic force modeling for milling of unidirectional carbon fiber reinforced polymer laminates. Int J Mach Tools Manuf 2012;56:79–93. https://doi.org/10.1016/j.ijmachtools.2012.01.001.